Chapter

CuO and MWCNTs Nanoparticles Filled PVA-PVP Nanocomposites: Morphological, Optical, Dielectric, and Electrical Characteristics

Hassan A.H. Alzahrani

Abstract

Copper dioxide (CuO) nanoparticles and multiwall carbon nanotubes (MWCNTs)-filled poly(vinyl alcohol) (PVA) and poly(vinyl pyrrolidone) (PVP) blend matrix (50/50 wt%)-based polymer nanocomposites (PNCs) have been prepared employing the solution-cast method. The X-ray diffraction explores the semicrystalline morphologies of these PNCs. The FTIR, SEM, and AFM measurements of PNCs expose the development of the miscible mix, polymer-polymer and polymer-nanoparticle interactions, and the influence of CuO and MWCNTs nanofillers on the morphology aspects on the main chain of PVA/PVP blend. The nanofiller loading for x = 14 wt% in the PVA–PVP blend matrix significantly enhances the crystalline phase, diminishing the optical energy gap to 2.31 eV. The DC conductivity is found to be maximum for x = 14 wt% loading concentration. The dielectric and electrical characteristics of these PNCs are investigated for an applied frequency range from 1 kHz to 1 MHz. The dielectric permittivity values increase substantially, owing to the decrease in the nano-confinement phenomenon at low frequency. The rise in applied frequency reduces dielectric permittivity and impedance values and enhances AC electrical conductivity. These PNCs having good dielectric and electrical characteristics can be used as frequency tunable nano-dielectric material in electronic devices.

Keywords: PVA, PVP, nanoparticles, nanocomposites, electrical properties, fillers

1. Introduction

Architectural polymers have become a subset of polymers with strong structural, optical, and electrical capabilities, outstanding geometrical durability, high weather resistance, and excellent fatigue strength [1–4]. This initiated the mixing of polymers, also known as polymer blending, a kind of engineering polymer that is similar to metallic ingots, and is created by combining at least two polymers to create a

separate material with varying basic properties [5–8]. The method of polymer blends includes melting, solvent blending, latex melding, partial blocking or grafting copolymerization, and the development of interpenetrating polymeric networks [9, 10]. Out of all previously stated, solvent blending is a very cost-effective and straightforward method of producing polymer mixtures. The solvent blending encompasses combining two or more polymers that are frequently immiscible and have compatible components. The interoperability should improve the frequency of the microstructures as well as the capabilities of the substance in terms of structural and bonding properties. In this regard, the poly(vinyl alcohol) (PVA) and poly(vinyl pyrrolidone) (PVP) mixture has developed remarkable qualities, including high elasticity, flexibility, nontoxicity, good mechanical strength, and thermal stability [11–13]. These configurations also have water-soluble, miscible, excellent electro-optic properties, and composite materializing attributes [2, 14]. Many investigators are involved in their research activities using PVA-PVP mixtures filled with nanoparticles to create a new polymer nanocomposite (PNCs) for any suitable technological applications [2, 15–17]. Because of their diverse advancement in different new tech, nanoparticles to be fully integrated into the polymer matrix, copper oxide (CuO), and multiwall carbon nanotubes (MWCNTs) have emerged as excellent nanofillers [18, 19]. The CuO nanoparticles belong to a class of transition metal oxide, with monoclinic structures and p-type semiconducting properties. These highly stable CuO nanofillers also have intriguing properties including outstanding thermophysical properties, good dispersion, photovoltaic capabilities, and antibacterial activity [19, 20]. Other nanofiller multiwall carbon nanotubes (MWCNTs), on the other hand, encompass many popped graphene sheets with structural complexity and variation. MWNTs, on the other hand, benefit from huge manufacturing facilities, low unit costs of production, improved thermodynamic features, and chemically resilient components. These MWCNTs can be used in sensitive gas detection materials, dielectric materials, and technologically challenging applications such as field emission and optoelectronic screens [14, 21–23]. This current chapter explores the fabrication of PVA-PVP: (15-x)CuO(x) MWCNTs nanocomposite by the means of solvent casting method for filler levels x = 0, 1, 5, 7.5, 10, 14, and 15wt percent. The preparation of composites by solvent casting method will have benefits such as uniform thickness, enhanced gloss, flexibility, low cost, and also no defects (die lines, extrusion, etc.). The fabricated PNCs are then investigated to explore the structural, optical, dielectric, and electronic properties of any potential device fabrication.

2. Experiments and results

In this current chapter, I have used CuO as one of the nanofillers. In the order to the synthesis of CuO nanofillers, I used crucial laboratory solution grades throughout the investigation. The required reagents (Cu ($C_2H_3O_2$)$_2$) and NaOH for the preparation were procured from Sigma-Aldrich, Germany. 0.02 mol of liquid copper acetate is treated with 1 ml glacial acetic acid. The combination is boiled at 110°C for 1 hour agitating with 500 rpm. 1 M NaOH acid is added to the sample outlined earlier, resulting in the formation of a dark cloud. Using a centrifuge, the precipitation caused by the mixture is retrieved to produce copper oxide nanofillers. This CuO aggregate is washed thoroughly with deionized water several times until all NaOH contaminants are removed until neutral pH values are achieved. The achieved CuO was then dried

for 8 hours in an oven at 500°C to remove the humidity component, yielding an approximate 94 percent.

On the other hand, nanofiller carbon nanotubes are considered due to unique properties such as enhanced configurability dispersal, compatibility, or reduced toxicity. 75 mg of multiwalled carbon nanotubes (MWCNTs with 3.5 nm diameter, 1–10m length, purity >90%, and specific surface area > 500 m2/g) was procured from Sigma-Aldrich and soaked in hydrochloric acid (HCl) for 24 hours. These soaked MWCNTs in HCl solution are mixed with 500 ml of distilled water and swirled for 20 minutes at a vigorous stirring rate of 500 rpm. The agitated blend was then screened through a Whatman Nylon filter membrane with a pore size of 0.1 m. The acquired remnant mixture is thoroughly treated until the pH level of the filtrated mixture is neutral. Following that, the MWCNTs were dried in a vacuum oven at 6000°C for 20 hours to remove the water component. Alternate MWCNTs were finely dispersed in a 3:1 volume proportion of sulfuric acid (H_2SO_4) and nitric acid (HNO_3) and homogenized for 2 hours using a probe ultrasonicator (PCI Analytics, India). After rinsing the dispersed mixture with distilled water until the filtrated solution is neutral, it is screened through a 0.1-m Whatman Nylon filter membrane. The precursor is cooked in a vacuum oven, and 73.2 mg of carboxylated MWCNTs (MWCNT-COOH) is produced.

PNCs are made by mixing 8 g of Mowiol 4–88 (PVA from Sigma-Aldrich, Germany, with a mean molecular weight of 31,000) with 80-ml deionized water and agitating for 60 minutes at 90°C to generate a transparent liquid. Similarly, 8 g of polyvinyl pyrrolidone (PVP, average molecular weight 40,000, Sigma Aldrich Germany) was combined with 80-ml deionized water. To make an acceptable liquid, this mixture is swirled for 2 hours at 70°C and 500 rpm. A motorized mixer was used to remix the clear, viscous liquid for 1 hour at room temperature (at 300 rpm). The resulting thick mixture is divided into eight equal parts. The following equation produces PVA-PVP:(15-x)CuO(x) MWCNTs nanocomposites with varied "x" nanofiller loadings:

$$x\% = \frac{W_d}{(W_d + W_p)}X100 \tag{1}$$

where W_d and W_p signify the weight of the embedded nanofillers and host polymer blend, respectively.

The synthesized ZnO and MWCNTs nanofillers with weights of x = 0, 1, 5, 7.5, 10, 14, and 15 have been embedded in the matrix. Moreover, ultrasonicator is utilized to fill the nanofillers in every region of the PVA-PVP mix for 10minutes or until all nanofillers are evenly disseminated. Each component of the PVA-PVP:(15-x)CuO(x) MWCNTs solution is put on a glassware petri-dish and dried overnight in an oven at 500°C. Each nanocomposite is scraped and wrapped in a silver sheet before being kept in a vacuum environment for further examination.

The prepared PNCs have a thickness of 165–180 nm predicted using a DektaK stylus profilometer (Bruker). The structural parameters of PNCs are established *via* Cu-K reflections (=15406A) by the Empyrean third-generation Malvern Panalytical X-ray Diffractometer. **Figure 1** depicts the XRD spectra of PVA-PVP:(15-x)CuO(x) MWCNTs at various loading levels of the "x" filled compound x = 0 to 1, 5, 7.5, 10, 14, and 15% wt. Filled MWCNTs exhibit a small uptick in the diffraction angle of MWCNTs at 26.52 degrees (JCPDS file no: 48–1449). Peaks at 2 = 21.6°, 29.7°, 36.5°, 42.4°, and 61.4°, which are comparable to (014), (111), (200), and (113), indicate the
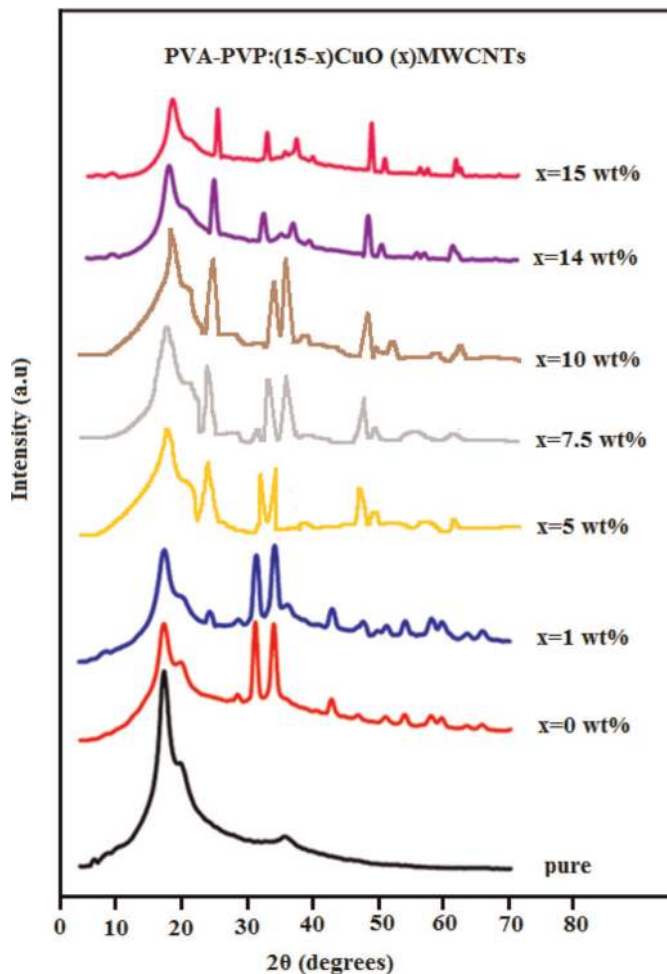
Figure 1.
XRD spectra of PVA-PVP:(15-x)CuO(x)MWCNTs PNCs.

presence of CuO nanoparticles. A broad, considerable rise is seen at scattering angles 19^0 to 20^0, which suggests the confirmation of the presence of a PVA semicrystalline peak (more precisely, of polyvinyl acetate). The PVP polymer long chain is indicated by the peak at 21.21^0, which corresponds to a d-value of 4.1544. Because of the incorporation of nanofillers, the breadth of semicrystalline peaks in PVA-PVP nanocomposite varies, revealing an increase in crystalline parameters. The strength of the crystallized spikes of PVA-PVP increases with filler level, and the results were mostly declared for filler level x = 14 percent. The OH group of the PVA-PVP backbone sequence and CuO/MWCNT nanofillers work together to improve complex conformation, resulting in crystalline phase gain. As the filler level rises, the PVA-PVP peaks shift to a lower angle.

   Table 1 also shows each microstructural strain (also referred to as strain), dislocation density (also referred to as density), and crystallinity (also known as phase) of PVA-PVP: (15-x)CuO(x)MWCNTs with varying filler dosage. The crystallite size in polymer nanocomposite evaluates molecular instability by integrating nanoparticles in the spine of the PVA-PVP polymer. We created an algorithm to describe the crystallinity behavior of composite materials using PowderX software (http://powdex. eng.umich.edu). The presence of intrinsic filler ions across the crystalline-state

Dopants concentrations (wt%)	% Crystallinity	D (nm)	Microstrain (ε) x 10^{-3}	δ (10^{16} lines/m^2)
Pure PVA-PVP	54.81	3.79	12.94	6.9618
0	53.96	9.89	4.313	1.022
1	55.01	10.06	4.224	0.988
5	56.03	10.91	3.780	0.840
7.5	57.12	11.78	2.133	0.720
10	57.67	12.52	1.997	0.637
14	58.92	13.88	1.487	0.519
15	56.71	12.59	1.812	0.630

Table 1.
Crystalline parameter values of PVA-PVP/(15-x)CuO(x)MWCNTs.

interstitial regions of the PVA-PVP backbone might be interpreted as a PVA main chain with nanofillers [24]. The "x" denotes filler weight concentration and for x = 14 percent, and the maximum crystallinity is observed. Recrystallization might play a significant role in the unexpected variation in defect characteristics of nanocomposites. Because of certain properties, the structural regularities of the PVA-PVP host molecule change when MWCNTs and CuO nanofillers are added. As a consequence, these factors improve the crystalline properties of PVA-PVP nanocomposites.

The occurrence of surface roughness as well as morphological changes in the filled composites was measured by the means of the solver-PRO (NT-MDT) AFM instrument. The tapping-mode AFM investigation evaluates the surface and roughness of the manufactured composites. **Figure 2(a)** and **(b)** shows two-dimensional (2D) AFM images of nanocomposite for unadulterated and optimal filler level x = 10wt percent. The root-medium-square (RMS) surface roughness of the composites is determined using the AFM topography in the scan region (**Table 2**). The RMS surface roughness
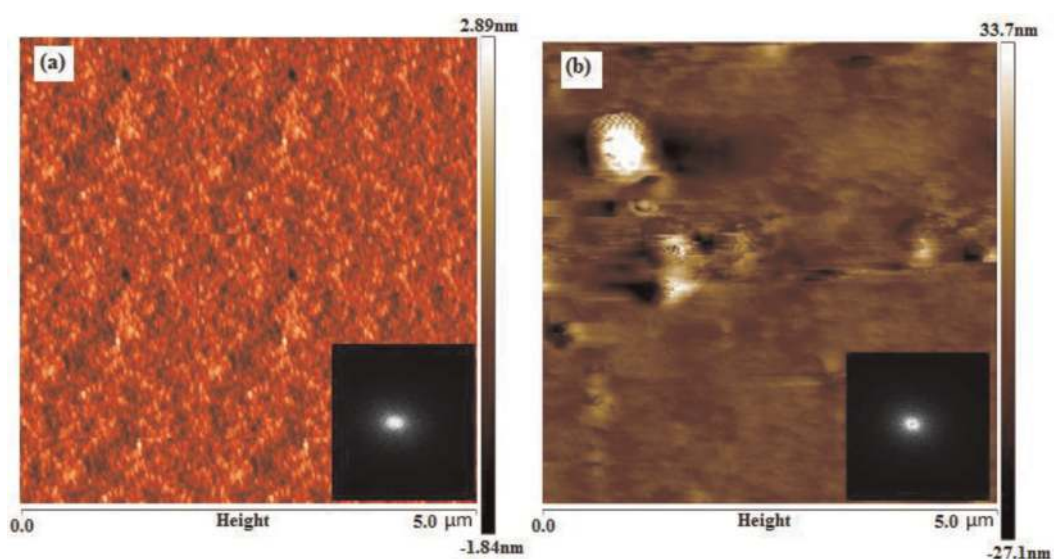

Figure 2.
AFM images (2D) with FFT transform spatial information of (a) pure PVA-PVP and (b) PVA-PVP with nanofillers for x = 14 wt% filler concentration.

Parameter	Mean	Minimum	Maximum	Sigma
Total count	8.000	8.000	8.000	0.000
Density	0.320 (/μm^2)	0.320 (/μm^2)	0.320 (/μm^2)	0.000 (/μm^2)
Height	14.508 (nm)	5.172 (nm)	42.576 (nm)	14.187 (nm)
Area	58031.082 (nm^2)	9536.743 (nm^2)	321960.438 (nm^2)	100274.750 (nm^2)
Diameter	216.134 (nm)	110.193 (nm)	640.260 (nm)	164.844 (nm)

Table 2.
AFM parameters of PVA-PVP:(15-x)CuO (x)MWCNTs of optimum filler loading x = 14 wt%.

measurements are 1.3 nm for x = 14 wt percent. The incorporation of nanofiller MWCNTs and CuO into the PVA-PVP mix improves the roughness of the RMS up to x = 14 wt percent loading. An improvement in the roughness indicates an improvement in the crystalline properties of nanocomposites. AFM images also display the linked images' quick two-dimensional fast Fourier transform (FFT). This 2-D FFT converts spatial info to frequency, which is highly valuable for analyzing the morphology of the nanocomposite surface. In the FFT images, the white dots represent the periodicity of surface morphology. The white point density is higher in the x = 14 wt percent filler level than in the pure PVA-PVP mix film. As a result, we may conclude that MWCNTs and CuO nanofillers are randomly oriented inside the PVA-PVP matrix, resulting in a large patch of scattered intensity at the center. **Figure 3** shows PVA-PVP 3-D photographs: (15-x)CuO (x)MWCNTs with x = 14 wt% nanofiller concentration. Within the PVA matrix, AFM suggests the particle heights of the order 33.7 nm having an average specific diameter of nearly 118.43 nm.

The cryo-scanning model SEM EVO 18 ALTO 1000 estimates the morphological structure, particle size estimation, and content of PNCs. **Figure 4** depicts SEM surface morphology, signposting both the nanofillers are equally dispersed in PVA-PVP for x = 14 wt%. It is also clear that the PVA-PVP combination shows the complex
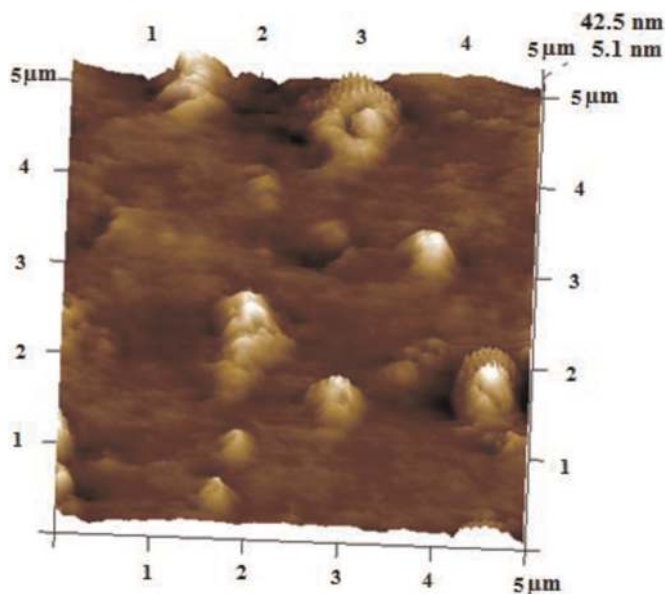
Figure 3.
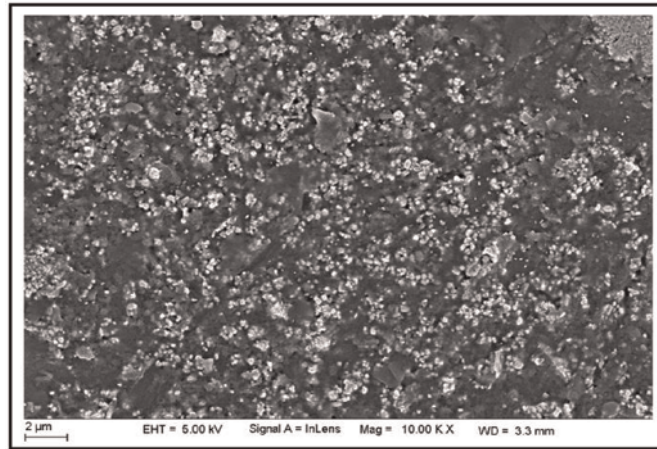*AFM 3-dimensional photograph of PVA-PVP (15-x)CuO(x)MWCNTs for x = 14 wt%.*

Figure 4.
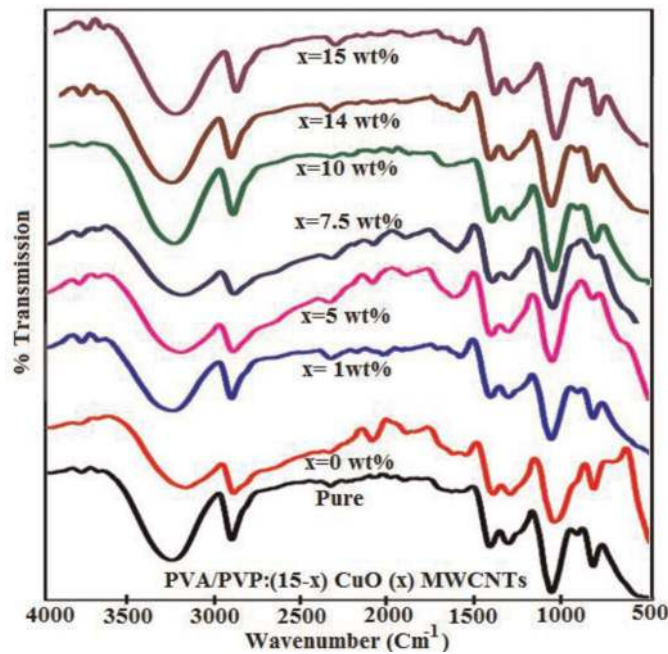*SEM photographs of PVA-PVP:(15-x)CuO(x)MWCNTs for x = 14 wt%.*

Figure 5.
FTIR spectra of PVP/PVA(15-x)CuO(x) MWCNTs PNCs.

entanglement with both added nanofillers CuO and MWCNTs, resulting in a homogeneous nanocomposite film. For optimal concentration x = 14wt percent, the entangling or binding between MWCNTs and CuO nanofillers is high. The high concentration of solely MWCNTs or CuO nanofillers restricts (x = 15wt percent or x = 0 wt percent) enhancement of the nanocomposites' structural behavior.

The FTIR spectra of PNCs are procured with 50 scans and 2 cm^{-1} precision using a KBr Pellets Varian Excalibur FTIR Spectrometer in the 500 to 4000 cm^{-1} range. In **Figure 5**, continuum demonstrated typical bending and stretching vibration of a structural class of constructed PVA-PVP:(15-x)CuO(x) MWCNTs PNCs. The presence of the O-H hydroxyl group in a pure PVP/PVA mix is indicated by the broad and extreme range peaks detected regularly at 2857–3631 cm^{-1}. The shifting of the O-H

band in the altered PVA-PVP mix corresponds to the amount of added nanofiller levels. The addition of filler up to x = 14wt percent changes the OH stretching frequencies to lower wavenumbers than pure PVA-PVP blends. The association of CuO and MWCNT nanofillers with the PVA/PVP-OH group is a key factor in enhancing the structural, optical, and electrical features. The narrowing of the hydroxyl band due to the nanofillers enhancement induces the semicrystalline in nanocomposite material. The rise in nanofillers leads to the OH vibrational bands of alcohol and phenols, at 3577 cm^{-1}, to shift toward the higher wavenumbers. In comparison with the pure PVA-PVP mix, the inclusion of nanofiller up to x = 14wt percent resulted in a shortening of the hydroxyl band. The peaks signifying at 2570 cm^{-1} represent a typical band of C-C oscillations of the PNCs. The primary chain PVA-PVP spectra are represented by three bands at 2492 and 2320, showing 141 cm^{-1} which shows the interaction of C-H symmetric distortion, CH_2 deformation, and C=O stretching with the loaded nanofillers [25]. The FTIR spectra show that the nanofillers CuO and MWCNTs move the several bands toward the lower frequency range. These modifications symbolize that the additional nanofillers entangle with C-H compounds in the PVA-PVP to generate complicated conformations [26]. An active absorption with band associated with symmetric and asymmetric stretching C=O of the PVA-PVP mix backbone structure originates at 1714–1011 cm^{-1}. The absorption peaks seen at 918 cm^{-1} indicate the PVA-PVP blend's syndiotactic structure. The addition of nanofillers improves the syndiotactic of the PVA-PVP mix, resulting in dense molecular packing and stronger intermolecular hydrogen bonding. These causes lead the molecular mobility to vanish, resulting in an increase in crystallinity inside the polymer matrix. Thus, the crystalline characteristics of PVP-PVA(15-x)CuO(x) MWCNTs PNCs were determined by the local surface chemistry, internal structural ordering of nanofillers, and strain engendered by nanofillers with the PVA-PVP host matrix.

Shimadzu UV-visible spectrometer is used to evaluate optical characteristics such as the energy gap of PVA-PVP (15-x)CuO(x) MWCNTs. **Figure 6** presents the UV-visible spectra of PNCs for varied dose amounts. The optical absorption coefficient increases as the loading dose increases. The intensity of the absorption bands increases with nanofiller content and exhibits redshifts, indicating an improvement in charge delocalization within the PVA-PVP network [27]. The formation of a complex
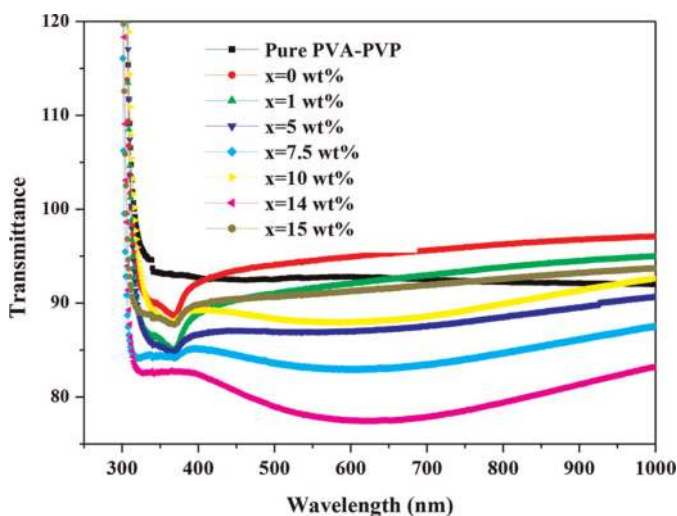

Figure 6.
UV-visible spectra of PVA-PVP:(15-x)CuO(x)MWCNTs PNCs.

between the host matrix and nanofillers enhances the shift in the absorption band. These intricate hydrophobic interactions increase nanofiller entanglement (complex conformation) with the host matrix, resulting in crystalline characteristics. The creation of complex conformation was found to be greatest until the filling level reached x = 10wt percent, modifying the wavelength of the absorption peaks and resulting in maximum absorption intensity. **Figure 7** exposes the indirect permitted transition of PNCs supplied by linear behavior at room temperature. The result of an extending of the linear component of the depicted curve from a measure of optical energy bandgap E_g of the PVA-PVP: (15-x)CuO (x) MWCNTs to $(hv)^{0.5} = 0$ is the optical energy bandgap E_g of PNCs. The graph depicts the respective bandgaps of PNCs for different loading levels. The reduction in the optical energy gap as filler loading increases for x = 10wt percent is due to nanofillers occupying interstitial locations between PVA-PVP chains and encouraging complex conformations [28]. This causes a charge exchange mechanism between the nanofillers and the PVA-PVP chain network, resulting in a smaller energy gap and increased conductivity in the PVA-PVP/(15-x) CuO(x) MWCNTs nanocomposites.

The DC electrical conductivity of MWCNT and CuO nanofillers (x = 0, 1, 5, 7.5, 10, 14, and 15wt percent) inside the PVA-PVP matrix is explored in **Table 3**. The DC
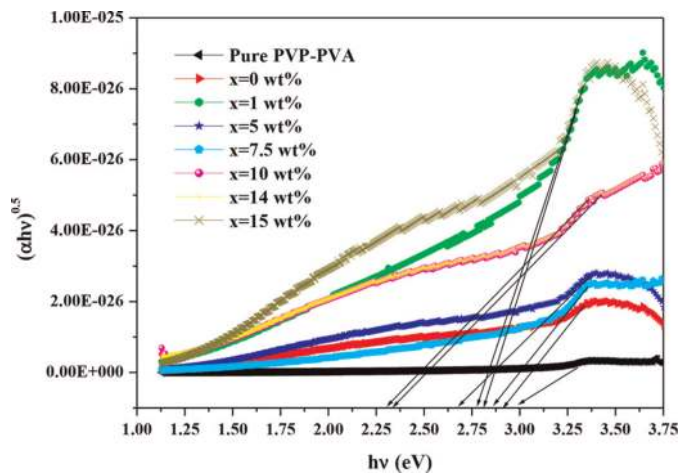

Figure 7.
Deviation of energy gap (E_g) for various loading levels.

Sl No	Filler concentration (wt%)	Resistance(Ω)	Conductivity (σ in S/cm)
1	Pure PVA-PVP	10.534×10^6	1.423×10^{-11}
2	0	9.337×10^6	1.605×10^{-11}
3	1	8.134×10^5	1.841×10^{-10}
4	5	7.970×10^5	1.882×10^{-10}
5	7.5	6.334×10^4	2.368×10^{-9}
6	10	2.943×10^4	5.096×10^{-9}
7	14	1.123×10^4	13.35×10^{-9}
8	15	2.278×10^4	6.584×10^{-9}

Table 3.
DC conductivity parameters of PVA-PVP:(15-x)CuO(x)MWCNTs PNCs.

conductivity of PNCs increases by 13.35 x 10^{-9} S/cm at nanoparticles volume fraction x = 14wt percent. The PVA-PVP chain network embedded with nanofillers promotes the charge transfer complexes within the nanocomposites (CTCs). The semicrystalline PVA-PVP nanocomposites that generate CTCs have an increased conductivity in amorphous regions of the polymer matrix as a consequence of reduced barrier heights. With a (bi) polaron wave function overlay on the PVA-PVP chain, rapid intrachain wavelike movement is made possible by the PVA-PVP network's PVA-PVP for electron conveyance. This fallout in leaping motion from site to site is initiated by the contacts of (bi)polaron with neighboring chains [29]. Fluctuations in carrier activity caused by nanofiller loading may lead to reduced activation energies. Interstitial PVA-PVP chains may include MWCNTs and CuO nanofillers, which may be considered to be dispersed throughout the amorphous phase. Hydrogen bonds between the nanofillers and the PVA-PVP chain conduct charge between the nanofillers and the PVA-PVP network. The interfacial barrier is increased and the likelihood of insulator chain transitions is decreased by lowering the crystalline-amorphous contact. This is explained by the percolation theory, which states that the nanoparticles create a conducting path between two charging sites.

Contrary to neutral conjugated polymers, counterions must be considered when transporters are included. There are (bi)polaron traps created by the coulomb interaction of counterions due to the low loading level. As the loading level is raised from x = 0 to 14%, coulomb traps are reduced, allowing the carriers to move inside and across chains. These traps overlap by decreasing the barrier and encouraging movement at x = 14wt percent ideal filled. Carrier transportation interchain is considerably affected by nanocomposites' shape and microstructure conditions that reduce conductivity above x > 14wt percent [30].

The thermal degradation at heating intervals of 10 °C/min is archived utilizing Shimadzu Thermogravimetric-45H in a temperature range of 35 to 650°C. **Figure 8** shows the thermal behavior of crucial PVP-PVA mix and filled PNCs with stages of loading x = 0,1,5,7.5,10,14, and 15wt. A considerable weight loss between 120°C and 255°C resulted in the fragmentation of macromolecular chains [31]. The thermal breakdown of the PVA-PVP main chains is responsible for the significant substantial weight loss over 260°C. In the majority of the experiments, a peak between 550 and
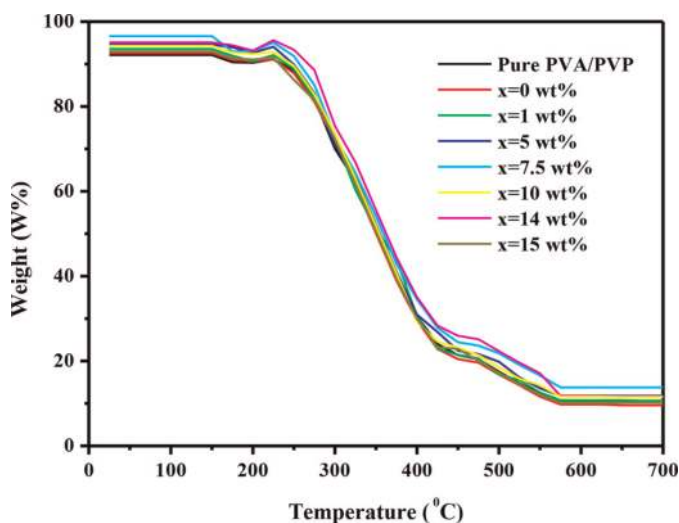

Figure 8.
TGA thermograms of PNCs for different filler levels.

650°C was discovered, which was attributed to carbonization and degradation of the polymer mixture [32]. Thermal stability is also improved by shifting the curves to higher temperatures and increasing the nanofiller loading levels. The improved thermal stability could be attributed to the superior thermal properties of the additional nanofillers, which promote heat dissipation in PVA-PVP matrices [33]. The interfacial contact and morphological variations inside the PNC for an optimal filler level x = 14 wt percent may promote heat dissipation and successfully postpone the disintegration of nanocomposites. The enhancement of the interfacial contact between embedded nanofillers and PVA-PVP PNCs dispersion up to x = 14wt percent loading promotes improvement in thermal stability when compared with pure PVA-PVP blend.

The TGA curves give the thermodynamics parameters obtained by employing the following two processes mainly Coats–Redfern method and the Broido method [34]. Determining the undecomposed initial "Y" number of molecules for different temperatures (T), a graph of ln [ln (1/Y)] versus 1/T shows a quite close straight path. Calculated slope using successive lines yields the activation energy [35]. **Table 4** shows how activation energy (E) measurements in Coats, Redfern, and Broido technique, reducing with the rise in nanofillers loading to the optimal loading value. This demonstrates the significant impact of the inclusion of nanoparticles in the polymer backbone of the PVA-PVP mix.

Fluorescence spectrophotometer-Cary eclipse (Varian) PL spectra are employed for determining the photoluminescent spectrum using emission and arousal slit size 5 nm, scanning rate 120 nm/min, data interval 1 nm (average time 0.5 s), PMT voltage 600 V, and exc = 325 nm wavelength by excitation. **Figure 9** signposts the photoluminescence of PVP/PVA(15-x)CuO(x) MWCNTs PNCs with a percentage loading levels for x = 0, 1, 5, 7.5, 10, 14, and 15wt. PL is an approach for measuring electrical properties that is influenced by the complex particles aspect created by crystallinity. At room temperature, PL studies for generated PNCs were performed at a surge wavelength of 375 nm. By ignoring a specified harmonic reflection order, the PNCs produce thrilling pinnacles at 380 nm and accurate, strong emission bands throughout the visual range of 650 nm [36]. The planar PVA-PVP polymer molecules are represented by the first strong PL in the near UV-vis regions. The electronic displacement of the OH side chain in the three distinct aqueous, isotactic, syndiotactic, and atactic polymer configurations corresponds to the broad emission

Nanofiller loading concentration "x" (wt%)	Coats–Redfern method (KJ/mol)	Broido method (KJ/mol)	Percentage crystallinity
Pure PVA-PVP	260.2	257.5	50.77
0	258.3	254.9	52.84
1	254.7	250.1	53.17
5	250.7	246.7	54.11
7.5	243.8	238.4	54.78
10	236.3	231.8	55.11
14	227.6	222.7	56.34
15	237.1	234.2	55.01

Table 4.
Activation energy and percentage crystallinity of unfilled and filled PNCs employing Coats–Redfern and Broido techniques.
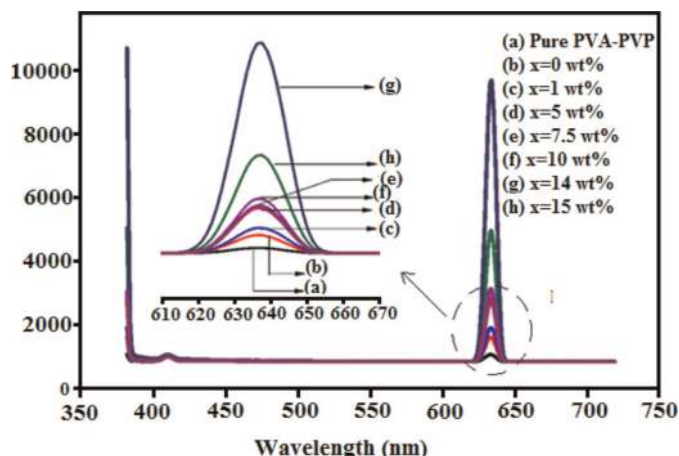
Figure 9.
PL spectra of synthesized PNCs.

spectrum discovered for PVA-PVP nanocomposite [37]. The electron-hole interaction of MWCNTs with CuO nanofillers is reminiscent of a pronounced emission band at 638 nm. Some scientists ascribe the wideband PL emission of PVP-PVA(15-x)CuO(x) MWCNTs nanocomposites to CuO structural deficiencies (green regions), such as oxygen vacancies, and MWCNTs, as well as specific contaminants (yellow and orange areas) [38].

PNCs real and complex dielectric nanocomposites are assessed utilizing the 4200-SCS Keithley parameter analyzer at rooms from 1 kHz to 1 MHz across frequency bands. The spectroscopy of complex dielectric permittivity (real part ε' and imaginary part ε'') and the dielectric loss tangent (tan δ) of PVA-PVP/(15–x)CuO (x) MWCNTs composites at variable doses at room temperature are shown in **Figures 10–12**. **Figure 10** shows how the PNCs ε' values decrease when the frequency is increased [39]. **Figure 10** shows that the ε' values of the unclassified PVA-PVP blend mix declined nonlinearly from 14.62 to 6.32 as the applied frequency increased from 1 kHz to 1 MHz, but the ε' values of PNCs dropped virtually consistently in the range
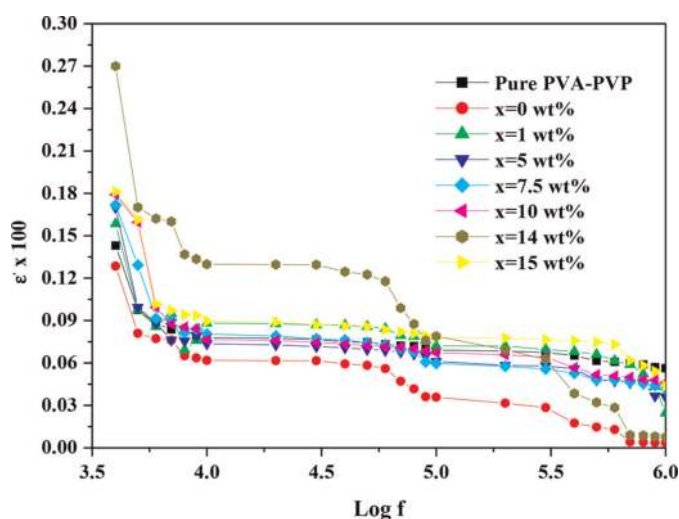

Figure 10.
Deviation of the real dielectric constant of PVA-PVP:(15-x)CuO(x)MWCNTs PNCs for different filler concentrations.
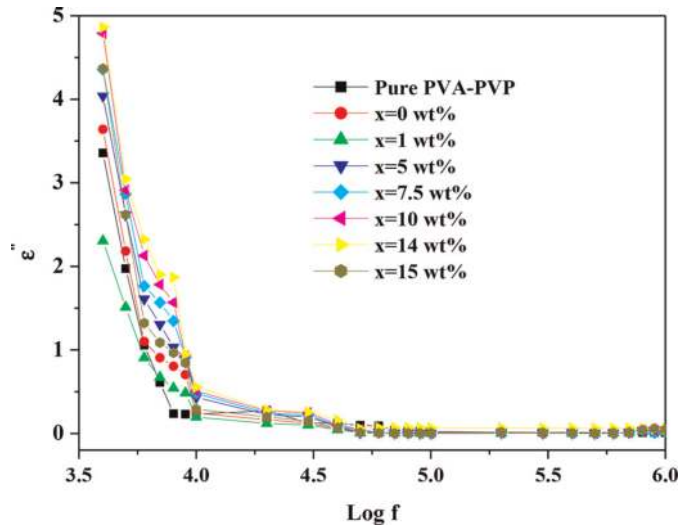
Figure 11.
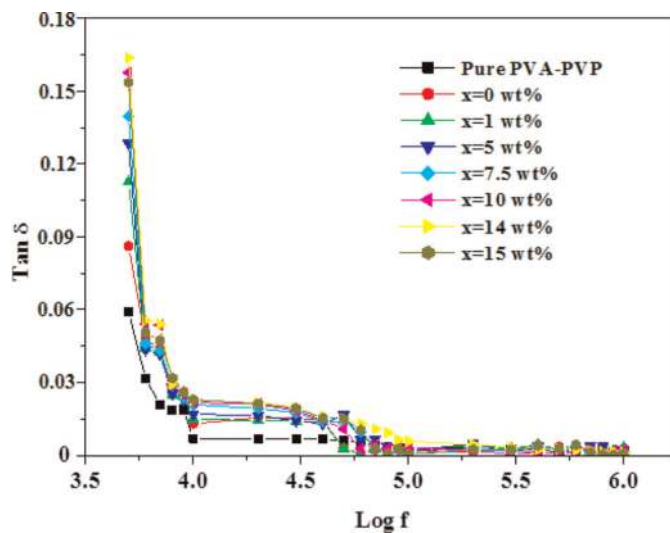*Variation of imaginary dielectric constant for different filler loadings.*

Figure 12.
Variation of tan δ versus frequency of PNCs.

26.97–2.81, indicating adjustable frequency response. The large drop in ε' values over the lower frequency range of x = 14 wt percent loading is proof of the nanoconfinement effect's major influence on the PVA-PVP network. The nanoconfinement effect is widely understood to be principally due to higher dipolar unit obstruction in the PVA-PVP network caused by nanofillers with a time-different electric field, which reduces the dipolar polarization of the PVP-PVA(15-x)CuO(x) MWCNTs PNCs [40]. The fact that the measurements of ε'' for PVP/PVA(15-x)CuO (x) MWCNTs PNCs for x = 14wt percent are similar to those of the other filler content nanocomposites demonstrates that the nanocontainment impact plays no effect in the higher-frequency dielectric polarization. In comparison with unfilled PVA-PVP mix film, the ε'' and Tan values in **Figures 11** and **12** declined significantly at low frequencies and displayed a rather stable behavior. The findings reveal that adding x = 14 wt% nanofiller to the PVA-PVP mix reduces low-frequency dielectric losses considerably.

Additionally, the ε'' values of PNC films have decreased significantly, with a further increase in loading level up to x = 14wt percent. For higher applied frequencies (i.e., f > 10 kHz), the ε'' and Tan δ values first declined considerably with the rise in frequency and then rose significantly. Throughout 1 kHz and 10 kHz, the ε'' and Tan δ spectra of PVP/PVA(15-x)CuO(x) MWCNTs nanocomposites show diminishing trends for x = 14wt percent loading level. Simultaneously, the dielectric relaxation frequency range between 10 kHz and 1 MHz decreases, leading to conductivity [41]. Thus, up to x = 14wt percent, these PNCs exhibit a steady gain in parameter values with an increase in frequency, and at higher applied frequencies, these composites demonstrate a dipolar relaxation process.

3. Conclusion

This chapter conveys the impacts of structural, optical, thermal, dielectric, and electrical properties of CuO nanoparticles and multiwall carbon nanotubes (MWCNTs)-filled PVA and PVP blend matrix (50/50wt percent) for x = 0,1,5,7.5, 10,14, and 15wt percent. For x = 14wt percent loading, X-ray diffraction research reveals an improvement in crystallinity of PNCs. The FTIR, SEM, and AFM measurements of PVA-PVP:(15-x)CuO (x)MWCNTs for x = 0,1,5,7.5, 10,14, and 15wt percent provide information on the miscible mix, PVA-PVP interaction and polymer-nanoparticle interfaces, and the influence of CuO and MWCNTs nanofillers on the morphology aspects of the PVA-PVP blend network. For optical investigations signposting for x = 14wt percent, the nanofiller dispersion in the PNCs matrix appreciably improves the crystalline phase, reducing the optical energy gap to 2.31 eV. The rise in optimal loading up to x = 14wt percent enhances the DC conductivity by 13.35x10–9 S/cm. Ignoring a certain harmonic order of reflection, photoluminescence investigations of PNCs show thrilling pinnacles at 380 nm and precise, strong emission bands throughout the visual range of 650 nm. TGA experiments exhibit that increasing the interface contact between MWCNTs with CuO nanofillers and PVA-PVP PNCs dispersion up to x = 14 wt% loading level may augment the thermal stability in comparison with pure PVA-PVP blend. The dielectric and electrical properties of these PNCs are examined over frequency ranges ranging from 1 kHz to 1 MHz. The establishment of a percolating network *via* the PNCs is caused by an increase in the nanofiller level up to x = 14wt percent in the PNCs matrix. Because of the reduction in the nanoconfinement phenomena, these variables significantly increase the dielectric permittivity values. As the applied frequency increases, the real sections of dielectric permittivity decrease and electrical conductivity increases. This PVA-PVP:(15-x)CuO (x)MWCNTs with excellent dielectric and electrical properties may be employed in electronic circuits as frequency adjustable dielectric PNCs.

Acknowledgements

Conflict of interest

The author declares no conflict of interest.

Author details

Hassan A.H. Alzahrani
Department of Chemistry, University of Jeddah, College of Science and Arts at Khulis, Jeddah, Saudi Arabia

*Address all correspondence to: hahalzahrani@uj.edu.sa

IntechOpen

References

[1] Demir MM, Memesa M, Castignolles P, Wegner G. PMMA/zinc oxide nanocomposites prepared by in-situ bulk polymerization. Macromolecular Rapid Communications. 2006;**27**(10):763-770

[2] Abdelrazek EM, Elashmawi IS, El-Khodary A, Yassin A. Structural, optical, thermal and electrical studies on PVA/PVP blends filled with lithium bromide. Current Applied Physics. 2010;**10**: 607-613

[3] Todd Alam M, Otaigbe JU, Rhoades D, Holland GP, Cherry BR, Kotula PG. Nanostructured polymer blends: Synthesis and structure. Polymer. 2005;**46**(26):12468-12479

[4] Baskaran R, Selvasekarapandian S, Kuwata N, Kawamura J, Hattori T. Conductivity and thermal studies of blend polymer electrolytes based on PVAc–PMMA. Solid State Ionics. 2006; **177**:2679-2682

[5] Kumar KK, Ravi M, Pavani Y, Bhavani S, Sharma AK, Narasimha Rao VVR. Investigations on PEO/PVP/NaBrcomplexed polymer blend electrolytes for electrochemical cell applications. Journal of Membrane Science. 2014;**454**:200-211

[6] Rithin Kumar NB, Acharya S, Alhadhrami A, Prasanna BM, Gurumurthy SC, Bhat S. Role of TiO$_2$/ZnO nanofillers in modifying the properties PMMA nanocomposites for optical device applications. Iranian Journal of Science and Technology, Transactions A: Science. 2021;**45**:2169-2179. DOI: 10.1007/s40995-021-01183-4

[7] Phiwdang K, Suphankij S, Mekprasart W, Pecharapa W. Synthesis of CuO nanoparticles by precipitation method using different precursors. Energy Procedia. 2013;**34**:740-745

[8] Rajeswari N, Selvasekarapandian S, Sanjeeviraja C, Kawamura J, Asath Bahadur S. A study on polymer blend electrolyte based on PVA/PVP with proton salt. Polymer Bulletin. 2014;**71**: 1061-1080

[9] Subba Reddy CV, Sharma AK, Narasimha Rao VVR. Electrical and optical properties of a polyblend electrolyte. Polymer. 2006;**47**:1318-1323

[10] Dai ZD, Ansaloni L, Gin DL, Noble RD, Deng LY. Journal of Membrane Science. 2017;**523**:551-560

[11] Yalagala B, Khandelwal S, Deepika J, Badhulika S. Wirelessly destructible MgO-PVP-graphene composite based flexible transient memristor for security applications. Materials Science in Semiconductor Processing. 2019;**104**: 104673

[12] Ali FM, Kershi RM, Sayed MA, Abou Deif YM. Evaluation of structural and optical properties of Ce3 + ions doped (PVA/PVP) composite films for new organic semiconductors. Physica B Condensed Matter. 2018;**538**: 160-166

[13] Mahendia S, Kandhol G, Deshpande UP, Kumar S. Determination of glass transition temperature of reduced graphene oxide-poly(vinyl alcohol) composites using temperature-dependent Fourier transform infrared spectroscopy. Journal of Molecular Structure. 2016;**1111**:46-54

[14] Bhajantri RF, Ravindrachary V, Poojary B, Harisha A, Crasta V. Studies on fluorescent PVA + PVP + MPDMAPP

composite films. Polymer Engineering and Science. 2009;**49**(5):903-909

[15] Azam A, Ahmed AS, Oves M, Khan MS, Memic A. Size-dependent antimicrobial properties of CuO nanoparticles against gram-positive and -negative bacterial strains. International Journal of Nanomedicine. 2012;**7**:3527-3535

[16] Peng X, Wong SS. Functional covalent chemistry of carbon nanotube surfaces. Advanced Materials. 2009; **21**(6):625-642. DOI: 10.1002/adma.200801464

[17] Jeyaraman R, Kadarkaraithangam J, Arumugam M, Govindasamy R, Abdul A. Synthesis and antimicrobial activity of copper nanoparticles. Materials Letters. 2011;**71**:114-116

[18] Liu Z, Jiao L, Yao Y, Xian X, Zhang J. Aligned, Ultralong single-walled carbon nanotubes: From synthesis, sorting, to electronic devices. Advanced Materials. 2010;**22**(21):2285-2310. DOI: 10.1002/adma.200904167

[19] Park SH, Lee WJ. Hierarchically mesoporous CuO/carbon nanofiber coaxial shell-core nanowires for lithium ion batteries. Scientific Reports. 2015;**5**:9754

[20] Sahooli M, Sabbaghi S, Saboori R. Synthesis and characterization of mono sized CuOnanoparticles. Materials Letters. 2012;**81**:169-172

[21] Zidan HM. Journal of Applied Polymer Science. 2003;**88**:1115-1120

[22] Rithin Kumar NB, Crasta V, Praveen BM. Enhancement of optical, mechanical and micro structural properties in nanocomposite films of PVA doped with WO3 nanoparticles. International Journal of Structural Integrity. 2015;**6**(3):338-354

[23] Hemanth Kumar GN, Lakshmana Rao J, Gopal NO, Narasimhulu KVC, Chakradhar RPS, Varada Rajulu A. Spectroscopic investigation Mn+2 ions doped polyvinyl alcohol films. Polymer. 2004;**45**:5407-5415

[24] Abdelrazek EM, Abdelghany AM, Oraby AH, Asnag GM. Investigation of mixed filler effect on optical and structural properties of PEMA films. International Journal of Engineering and Technology. 2012;**12**:98-102

[25] Saini I, Rozra J, Chandak N, Aggarwal S, Sharma PK, Sharma A. Tailoring of electrical, optical and structural properties of PVA by adding Ag nanoparticles. Materials Chemistry and Physics. 2013;**139**:802-810

[26] Davis EA, Mott NF. Conduction in non-crystalline systems. V. Conductivity, optical absorption and photoconductivity in amorphous semiconductors. Philosophical Magazine. 1970;**22**:0903-0922

[27] Mott NF. Conduction in non-crystalline systems: IV. Anderson localization in a disordered lattice. Philosophical Magazine. 1970;**22**:7-29

[28] Collins BA, Cochran JE, Yan H, Gann E, Hub C, Fink R, et al. Polarized X-ray scattering reveals non-crystalline orientational ordering in organic films. Nature Materials. 2012;**11**:536-543

[29] Noriega R, Rivnay J, Vandewal K, Koch FP, Stingelin N, Smith P, et al. A general relationship between disorder, aggregation and charge transport in conjugated polymers. Nature Materials. 2013;**12**:1038-1044

[30] Kang SD, Snyder GJ. Charge-transport model for conducting polymers. Nature Materials. 2017;**16**: 252-257

[31] Patel SN, Glaudell AM, Peterson KA, Thomas EM, O'Hara KA, Lim E, et al. Morphology controls the thermoelectric power factor of a doped semiconducting polymer. Science Advances. 2017;**3**: e1700434

[32] Kim H-S, Yang H-S, Kim H-J, Park H-J. Journal of Thermal Analysis and Calorimetry. 2004;**76**:395-404

[33] Zuo G, Liu X, Fahlman M, Kemerink M. High Seebeck coefficient in mixtures of conjugated polymers. Advanced Functional Materials. 2018;**28**: 1703280

[34] Coats AW, Redfern JP. Nature. 1964; **201**:68-69

[35] Broido A. Journal of Polymer Science: Part A. 1969;**2**(7):1761-1773

[36] Gananatha Shetty B, Crasta V, Rithin Kumar NB, Rajesh K, Bairy R. Parutagouda Shankaragouda Patil, promising PVA/TiO2, CuO filled nanocomposites for electrical and third order nonlinear optical applications. Optical Materials. 2019;**95**:109218. DOI: 10.1016/j.optmat.2019.109218

[37] Mora ES, Barojas EG, Rojas ER, Gonzalez RS. Solar Energy Materials & Solar Cells. 2007;**91**:1412-1415

[38] Mazzera M, Zha M, Calestani D, Zappettini A, Lazzarini L, Salviati G, et al. Nanotechnology. 2007;**18**:355707

[39] Rithin Kumar NB, Crasta V, Praveen BM. Dielectric and electric conductivity studies of PVA (Mowiol 10-98) doped with MWCNTs and WO_3 nanocomposites films. Materials Research Express. 2016;**3**(5):055012

[40] Mardare D, Rusu GI. Comparison of the dielectric properties for doped and undoped TiO_2 thin films. Journal of Optoelectronics and Advanced Materials. 2004;**6**:333-336

[41] Rao V, Ashokan PV, Shridhar MH. Studies of dielectric relaxation and a.c. conductivity in cellulose acetate hydrogen phthalate-poly (methyl methacrylate) blends. Materials Science and Engineering A. 2000;**281**:213-220